DNA Secondary Structure and Raman Markers of Supercoiling in *Escherichia coli* Plasmid pUC19[†,‡]

Doinita Serban, James M. Benevides, and George J. Thomas, Jr.*

Division of Cell Biology and Biophysics, School of Biological Sciences, University of Missouri−Kansas City, Kansas City, Missouri 64110-2499

Received May 16, 2001; Revised Manuscript Received November 13, 2001

ABSTRACT: Negative supercoiling in the 2686 bp *Escherichia coli* plasmid pUC19 is comparable in linking number ($Lk_0 = 258$) and superhelical density ($\sigma = -0.05$) to the moderate supercoiling exhibited by many eukaryotic chromosomal DNAs in vivo. Supercoiled and relaxed forms of purified pUC19 in aqueous solution (0.1 M NaCl, pH 8.3, 20 °C) have been investigated by Raman spectroscopy to assess changes in B-DNA secondary structure induced by superhelical stress and to identify putative Raman markers of DNA supercoiling. We find that supercoiling leads to small but significant changes to the B-form Raman signature of linear DNA. Spectral band shifts in the 780−850 cm^{-1} interval are interpreted as resulting from a small net change in the average phosphodiester torsions α (O3′−P−⟩−O5′−C5′) and ζ (C3′−O3′−⟩−P−O5′) from the *gauche*$^-$/*gauche*$^-$ range to the *gauche*$^-$/*trans* range with supercoiling. The magnitude of the spectral intensity change implies that approximately 5% of the nucleotide moieties are affected. Supercoiling also introduces small redistributions of Raman intensity within the 1460−1490 and 1660−1670 cm^{-1} intervals, consistent with small structural perturbations. Importantly, no Raman markers of Watson−Crick base pairing, base stacking, or C2′-*endo*/*anti* deoxynucleoside conformations are perturbed significantly by supercoiling of pUC19, indicating that the B-DNA structure is largely conserved under moderate superhelical stress. Peak and trough features at 814 and 783 cm^{-1}, and at 1462 and 1489 cm^{-1}, respectively, in the Raman difference spectrum between superhelical and relaxed DNA are proposed as markers of moderate negative supercoiling. We also show that in Tris-buffered solutions the Raman signature of supercoiled DNA can be obscured by Raman bands of Tris counterions. The subtle structural perturbations to B-DNA induced by moderate supercoiling are consistent with proposed mechanisms of transcriptional activation.

Molecular mechanisms of genome replication, recombination, transcription, repair, and condensation all involve supercoiled states of DNA. Supercoiling, which can be either negative (underwinding) or positive (overwinding), is a structural adjustment that reduces stress without cleaving the covalently closed double-stranded (ds)[1] DNA molecule (*1*). The thermodynamic parameter relevant to supercoiling is the Gibbs free energy (ΔG_{Lk}), which is associated with the difference (ΔLk) between linking numbers of the supercoiled (Lk) and relaxed (Lk_0) forms of DNA. The linking number represents the number of times one strand of the duplex crosses the other. Supercoiling may also be characterized in terms of the superhelical density parameter, σ ($\equiv \Delta Lk/Lk_0$). Coupling of ΔG_{Lk} (or σ) to DNA unwinding is considered the rate-limiting step in many gene regulatory mechanisms (*2*).

DNA supercoiling has been investigated using a variety of biochemical and biophysical methods. Reviews have been done by Wells (*3*) and Strick and co-workers (*4*). Thermodynamic aspects of DNA supercoiling have also been investigated in detail (*1*). Experimental studies involving chemical probes, nuclease digestions, small-molecule binding assays, and cross-linking (*3*) provide evidence of either local denaturations or transitions to alternative secondary structures, such as A-DNA, Z-DNA, or cruciforms (*5*, *6*). However, structural details of supercoiled DNA at the nucleotide level remain largely unknown, because of the difficulties of applying high-resolution structural methods to conformationally strained DNA molecules.

Here, we investigate the structure of supercoiled DNA using Raman spectroscopy. The Raman spectrum has the capability of providing information about both local and global structures of large DNA molecules in solution under physiological conditions (*7*). Recent improvements in Raman difference methods also provide unprecedented sensitivity for comparing vibrational signatures of DNA in supercoiled and relaxed states. The effectiveness of Raman difference spectroscopy in distinguishing DNA conformational variants

[†] Supported by NIH Grant GM54378.

[‡] Part LXXIX in the series Raman Spectral Studies of Nucleic Acids.

* To whom correspondence should be addressed. Telephone: (816) 235-5247. Fax: (816) 235-1503. E-mail: thomasgj@umkc.edu.

[1] Abbreviations: CD, circular dichroism; dA, deoxyadenosine; dC, deoxycytidine; dG, deoxyguanosine; dT, thymidine; ds, double-stranded; IHF, integration host factor; LEF-1, lymphoid enhancer-binding factor-1; MOPS, morpholinopropanesulfonic acid; SDS, sodium dodecyl sulfate; Tris, tris(hydroxymethyl)aminomethane; Lk, linking number of supercoiled DNA; Lk_0, linking number of relaxed DNA; ΔLk, difference between linking numbers of supercoiled and relaxed DNA; σ, superhelical density of DNA ($=\Delta Lk/Lk_0$); $\Delta\epsilon$, molar ellipticity; θ, helical rotation angle of DNA; ΔG_{Lk}, free energy of DNA supercoiling; *g*, *gauche*; *t*, *trans*.

10.1021/bi011004z CCC: $22.00
Published on Web 12/27/2001

has been well documented (*8*−*11*) and reviewed recently (*12*, *13*). In the study presented here, we have examined the 2686 bp plasmid pUC19 in linear and negatively supercoiled forms ($\Delta Lk = -15$, $\sigma = -0.05$) (*14*). The level of supercoiling of many eukaryotic DNAs in vivo is believed to be similar to that of pUC19 in vivo.

The results of this study show that the solution structures of a supercoiled and linearized plasmid can be distinguished by Raman spectroscopy. The conformational differences observed at the nucleotide level are subtle but significant, and can be interpreted in terms of the phosphodiester torsions α (O3′−P−〉−O5′−C5′) and ζ (C3′−O3′−〉−P−O5′) of the DNA backbone. The structural consequences of supercoiling appear to be restricted mainly to the DNA backbone, whereas base pairing and base stacking remain largely unperturbed. The results obtained here are compared with the results of previously reported Raman studies of other DNA plasmids (*15*−*18*) and are also discussed in relation to the results of recent Raman studies of protein-directed DNA curvature (*19*, *20*). Additionally, the effects of buffers and counterions on the Raman signatures of supercoiled and relaxed DNA are considered (*21*).

MATERIALS AND METHODS

Preparation and Purification of Plasmid pUC19. *Escherichia coli* strain DH5-α and the transforming plasmid pUC19 were obtained from Sigma Chemical Co. (St. Louis, MO). The transformed cells were cultured in a Mobile Pilot Plant fermenter with a working volume of 30 L (New Brunswick Scientific, Edison, NJ) (*22*), pelleted in a Beckman Avanti J-20 centrifuge at 6000 rpm (8900*g*) for 10 min using a JLA-8.1 rotor, and resuspended in 50 mM Tris buffer (pH 8) containing 10 mM EDTA and 100 μg/μL RNase A.

The negatively supercoiled pUC19 plasmid was isolated from the suspension using the Qiagen (Valencia, CA) Endo Free Plasmid Giga Kit and a modified version of the Qiagen-patented protocol for production and purification of high-copy number plasmids. Briefly, the procedure involves modified alkaline lysis with NaOH and SDS and binding of the plasmid from the lysate to a DEAE-silica-based resin under specified conditions [50 mM MOPS (pH 7.0), 750 mM NaCl, and 15% 2-propanol]. RNA, proteins, carbohydrates, and low-molecular weight impurities were washed from the column with a medium-salt buffer [50 mM MOPS (pH 7.0), 1.0 M NaCl, and 15% 2-propanol], and the plasmid was eluted with a high-salt buffer [50 mM MOPS (pH 7.0), 1.6 M NaCl, and 15% 2-propanol]. The eluted plasmid was concentrated 200-fold on a Centriplus-100 ultrafiltrator with a 100 000 Da molecular mass cutoff (Amicon, Inc., Beverly, MA) and washed successively with pH 8.3 aqueous solutions containing 2.0 M NaCl and 0.1 M NaCl but no Tris. [An alternative procedure in which the eluted plasmid was washed initially with 10 mM Tris (pH 8.0) consistently led to the appearance of interfering Raman bands of the Tris cation in the DNA Raman spectra. Accordingly, Tris was not used in the final protocols for Raman sample preparations. See also Contributions of the Tris Cation to the Raman Spectrum of DNA (below).] All DNA solutions maintained a pH value of 8.3 ± 0.2 following completion of data collection protocols. The purity of the plasmid DNA was also assessed by agarose gel electrophoresis and ethidium bromide staining, and the absence of RNA and protein contaminants was confirmed by Raman spectroscopy. The linear form of the pUC19 plasmid was obtained by *Eco*RI digestion of the supercoiled form. The linearized DNA was purified by successive washings with saline solutions, as indicated above.

The restriction endonuclease (*Eco*RI) was obtained from New England Biolabs (Beverly, MA). Buffers (Tris and MOPS), ethidium bromide, agarose, and other reagents were obtained from Sigma. DNA concentrations were determined by UV absorbance measurements using a Cary 3E spectrophotometer (Varian, Inc., Palo Alto, CA) and a molar extinction coefficient at 260 nm (ϵ_{260}) of 3.5×10^7 M^{-1} cm^{-1} (*23*).

Raman Spectroscopy. Raman spectra of supercoiled and linear forms of pUC19 were measured over the concentration range of 10−50 μg/μL and showed no concentration dependence. Spectra shown below were obtained from solutions in which the supercoiled or linearized plasmid was dissolved to a final concentration of 25 μg/μL in 0.1 M NaCl (pH 8.3). Aliquots (∼5 μL) were sealed in a glass capillary (KIMAX no. 34507, 1.0 mm inside diameter), and the capillary was mounted in the thermostated (20 °C) sample illuminator of the Raman spectrophotometer (*24*). Spectra were excited at 532 nm using a solid-state Nd:YVO_4 laser (Verdi, Coherent, Inc., Santa Clara, CA). Raman scattering at 90° was collected on a Spex 500 M single spectrograph (Instruments S.A., Edison, NJ) equipped with a holographic notch filter and liquid nitrogen-cooled, back-thinned, charge-coupled-device detector of 2000 × 800 pixels (Spectrum One, Instruments S.A.). The radiant power at the sample was approximately 30 mW. The effective spectral resolution was 3 cm^{-1}. Raman frequencies, accurate to ±0.5 cm^{-1}, were calibrated using the 459.5 cm^{-1} band of CCl_4. Spectra shown below are accumulated averages of 10−30 exposures of 40 s each. Further details of the instrumentation and data collection protocols are given elsewhere (*25*).

Raman measurements comparing supercoiled and linearized topoisomers of pUC19 were repeated on three sets of independently prepared samples, each in 0.1 M NaCl (pH 8.3). An additional confirmatory data collection was also carried out on supercoiled and linearized pUC19 samples dissolved in D_2O solution [0.1 M NaCl (pD 8.3)].

Circular Dichroism Spectroscopy. CD spectra were obtained at 21 °C on DNA samples dissolved to a final concentration of ∼0.2 μg/μL in a 0.1 M NaCl solution (pH 8.3) using a Jasco J-720 spectropolarimeter (Japan Spectroscopic, Co., Tokyo, Japan) and an optical path length of 0.1 cm. Spectra shown below are the accumulated averages of 10 scans, each recorded at a scan rate of 0.5 nm/s. The instrument was calibrated using ammonium *d*-camphor-10-sulfonate.

Gel Electrophoresis. DNA samples (0.5−3 μg) were loaded on 1.2% (w/v) agarose gels. The gels were run in standard Tris-borate-EDTA buffer at room temperature, using an electric field strength of 1 V/cm. After being stained with ethidium bromide, the gels were illuminated with ultraviolet radiation and photographed with a Polaroid MP-4 camera (*23*).

RESULTS

Electrophoretic Mobility of pUC19 DNA. Relaxed (Lk_0) and supercoiled ($|Lk| \neq Lk_0$) DNA tertiary structures are

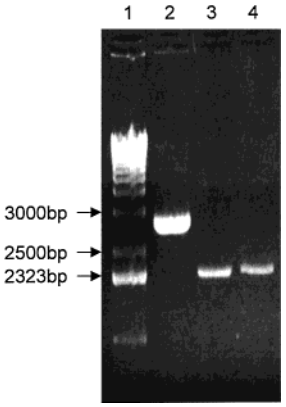

FIGURE 1: Agarose gel (1.2% w/v) electrophoresis of linearized and supercoiled forms of the 2686 bp pUC19 plasmid used for Raman spectroscopy. Lanes 1−3 contain DNA standards, linearized pUC19, and supercoiled pUC19, respectively. The profile of lane 3 was not significantly altered by the laser-Raman excitation and data collection protocol, as shown in lane 4.

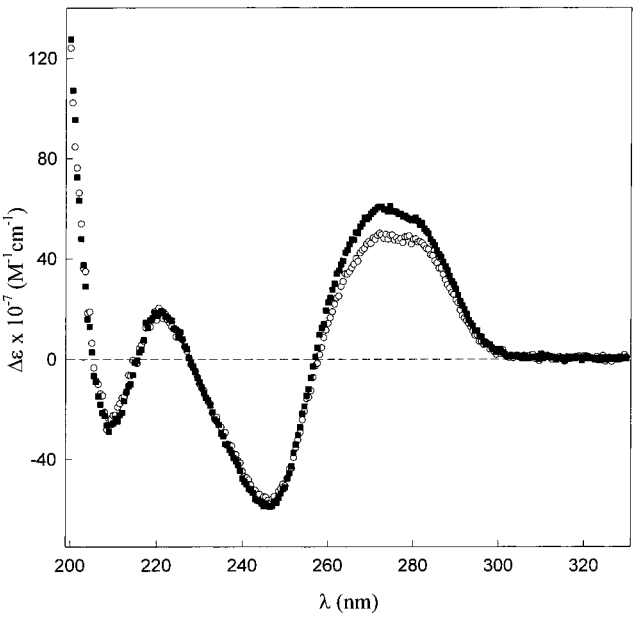

FIGURE 2: CD spectra of solutions of supercoiled (■) and linearized (○) forms of pUC19 at 2 mg/mL in 0.1 M NaCl at pH 8.3 and 20 °C.

readily distinguished by agarose gel electrophoresis (*26*), as shown in Figure 1. Whereas the *Eco*RI-linearized pUC19 plasmid migrates as expected to a position between the 2500 and 3000 bp standards (Figure 1, lane 2), the supercoiled topoisomer ($\sigma = -0.05$) exhibits significantly greater electrophoretic mobility, equivalent to that of linear DNA of ~2300 bp (Figure 1, lane 3). This is consistent with results reported for other supercoiled plasmids (*14*). The enhanced electrophoretic mobility of supercoiled DNA compared to that of relaxed DNA is explained by the more compact shape of the former (*6*).

CD Spectra of Supercoiled and Linearized pUC19 DNA. The CD spectrum, which is highly sensitive to DNA helical parameters, is perturbed significantly by supercoiling (*27*). CD spectra (200−330 nm) of supercoiled and linearized forms of pUC19 are shown in Figure 2. Although both forms exhibit the conservative profile of B-DNA, the ellipticity near 277 nm ($\Delta\epsilon_{277}$) is ~20% greater for the negatively supercoiled plasmid. CD studies of other plasmids indicate that

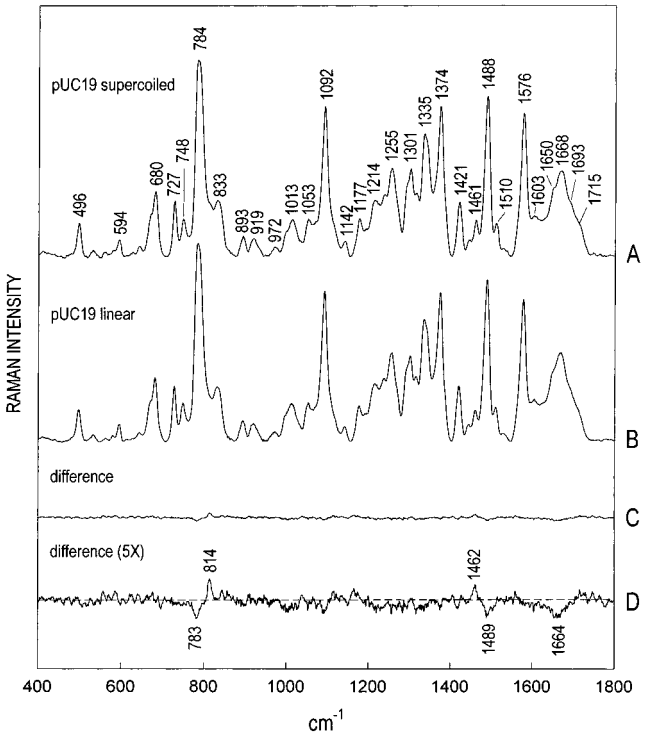

FIGURE 3: Raman spectra (400−1800 cm^{-1}, 532 nm excitation) of solutions of supercoiled (A) and linearized (B) forms of pUC19 at 25 mg/mL in 0.1 M NaCl at pH 8.3 and 20 °C, (C) their computed difference spectrum (spectrum C = spectrum A − spectrum B), and (D) a 5-fold amplification of the difference spectrum. Spectra A and B were normalized to the integrated intensity of the purine marker at 1576 cm^{-1}, as discussed in the text.

$\Delta\epsilon_{277}$ increases linearly with supercoiling for superhelical densities within the range of −0.05 to 0.05. This has been attributed to the change in average helical rotation angle ($\Delta\theta$) associated with negative supercoiling (*1*, *18*). On the basis of the relationship between $\Delta\epsilon_{277}$ and σ calculated by MacDermott et al. (*47*), we estimate that the observed $\Delta\epsilon_{277}^{\text{supercoil}}/\Delta\epsilon_{277}^{\text{linear}}$ ratio of 1.1 ± 0.05 for pUC19 (Figure 2) corresponds to a σ of −0.05 ± 0.007. Given that $\sigma \equiv \Delta Lk/Lk_0$ and $Lk_0 = N/10.4$ (*1*), where $N = 2686$ bp (*14*), we obtain a ΔLk of −13 ± 1.7. The supercoiling-induced changes in helical twist angle (ΔTw) and $\Delta\theta$ are interdependent [$\Delta\theta = (360\Delta Tw)/N$], as are ΔTw and ΔLk [$\Delta Tw = \Delta Lk - Wr$, where the writhe Wr (=0.72ΔLk) is independent of σ] (*1*, *6*). Accordingly, the CD data of Figure 2 indicate for pUC19 a decrease in the average helical rotation angle ($-\Delta\theta$) of 0.49 ± 0.05°.

The similar CD profiles of supercoiled and linearized forms of pUC19 indicate that supercoiling introduces little change to the average B-form secondary structure of the duplex. In particular, the absence of any significant wavelength shift in the ellipticity minimum (245 nm) or maximum (270 nm) of Figure 2 and the near-conservative profiles for both forms demonstrate that such alternative secondary structures as A- and Z-DNA are absent from the supercoil.

Raman Spectra of Supercoiled and Linearized pUC19 DNA. Raman spectra (400−1800 cm^{-1}) of supercoiled and linearized pUC19 are compared in Figure 3, using the purine marker at 1576 cm^{-1} for intensity normalization. The integrated intensity of the 1576 cm^{-1} band is known to be largely invariant to transformations between different double-

Table 1: Raman Band Frequencies, Intensities, and Assignments of pUC19 DNA

wavenumber (cm^{-1})	relative intensity (arbitrary units)[a]	assignment[b]
496	2.3	$\delta(PO_2^-)$
643	0.7	dC
670	2.9	dT
680	4.5	dG
727	3.8	dA
748	2.6	dT
784	13.6	dT, dC, bk
833	3.8	ν(OPO)
893	1.4	d
919	1.2	d
972	0.6	d
997s	1.7	d
1013	2.5	dT, dG, dC
1053	2.6	ν(CO)
1092	10.4	$\nu(PO_2^-)$
1142	1.0	dT
1177	2.6	dG
1189	1.8	dT, dC
1214	3.9	dC, dT
1237	4.3	dT, dC
1255	6.0	dA, dC
1292s	5.0	dC
1301	6.1	dA
1315	4.4	dG
1335	8.5	dA, dG
1374	10.4	dT, dA, dC
1421	3.7	d[δ(C2′H_2)], dA
1445	1.1	d[$\delta(CH_2)$]
1461	2.5	d[δ(C5′H_2)]
1488	11.1	dG, dA
1511	2.3	dA
1531	0.5	dC
1576	10.0	dG, dA
1603	2.7	dC, dG, dA
1650	4.8	dC, dT
1668	5.9	dT
1693s	3.6	dG
1715	2.1	dG

[a] Based upon 10.0 for the 1576 cm^{-1} band as the intensity standard (see the text). [b] Abbreviations: ν and δ, stretching and deformation vibrations, respectively, of the indicated atomic groups; bk, vibration of the DNA backbone; d, vibration localized in the deoxyribose moiety; dA, dT, dG, and dC, vibrations of the deoxynucleosides, including modes localized in either the purine or pyrimidine base or delocalized (base plus furanose moieties). Further details of vibrational assignments are given in refs *7*−*13*, *28*−*36*, *44*, *and 45* and citations therein.

helical forms of DNA (*8*, *9*, *28*) and to changes in solvent environment that do not lead to DNA denaturation (*29*, *30*). The phosphodioxy (PO_2^-) marker band at 1092 cm^{-1} is sometimes used for intensity normalizations in studies of DNA denaturation (*25*, *31*, *32*). The data of Figure 3 show that the intensities of both the 1092 and 1576 cm^{-1} markers are largely conserved with supercoiling. The Raman spectrum of the pUC19 plasmid is comparable to that of *E. coli* genomic DNA with which it shares 50% GC content (*30*). Importantly, the spectrum of the supercoil (Figure 3, trace A) exhibits signal-to-noise quality far superior to any reported previously for a supercoiled DNA (*15*−*18*).

Figure 3 shows that Raman signatures of the supercoiled (trace A) and linearized (trace B) plasmids are similar and typical of B-DNA. Raman bands and assignments are summarized in Table 1. Key structural markers occur at (i) 790 and 833 cm^{-1}, diagnostic of phosphodiester torsions α/ζ in the *gauche*$^-$/*gauche*$^-$ range (*25*, *32*, *33*); (ii) 680 cm^{-1},

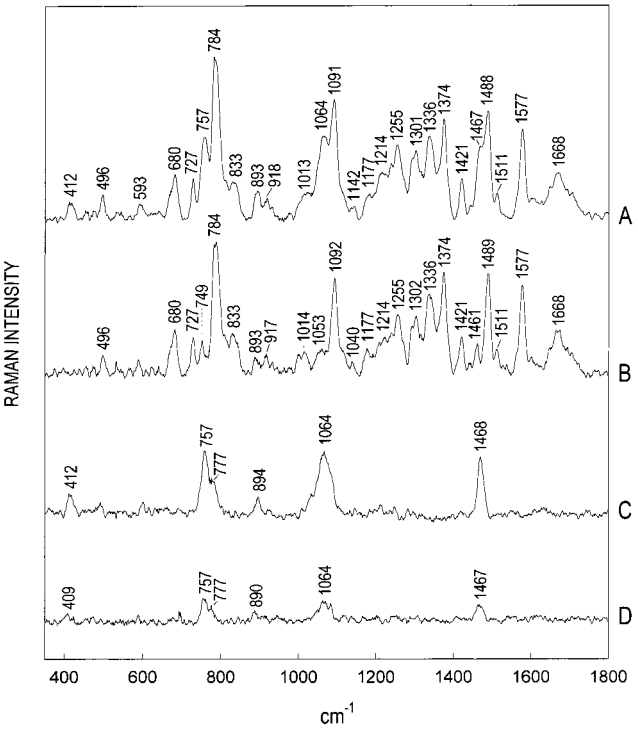

FIGURE 4: Contributions of the Tris cation to the Raman spectrum of pUC19 DNA. (A) Spectrum of supercoiled pUC19 at 25 mg/mL in 10 mM Tris-HCl at pH 8.3. (B) Spectrum of pUC19 from panel A after washing with 2 M NaCl and resuspension in 0.1 M NaCl and H_2O at pH 8.3. (C) Observed difference spectrum (spectrum C = spectrum A − spectrum B). (D) Raman spectrum of 10 mM Tris-HCl at pH 8.3.

diagnostic of C2′-*endo* sugar pucker and *anti* glycosyl torsion (*28*, *34*); and (iii) 1421 cm^{-1}, indicative of C2′H_2 moieties in the B-DNA conformation (*35*). The Figure 3 difference spectrum (trace C) demonstrates that negative supercoiling ($\sigma = -0.05$) does not radically alter the B-DNA conformation. However, small responses to superhelical strain are clearly evident in the amplified difference spectrum (Figure 3, trace D, which is interpreted in detail in the Discussion). The absence of positive difference bands in the 600−800 and 1200−1400 cm^{-1} intervals of Figure 3 and the small amplitudes of changes in the 1500−1800 cm^{-1} interval indicate that Watson−Crick base pairing and base stacking of B-DNA are not perturbed significantly by supercoiling (*25*, *31*, *33*−*36*).

Contributions of the Tris Cation to the Raman Spectrum of DNA. As noted above (Materials and Methods), the Raman spectra reported here for supercoiled and linearized DNA were obtained from solutions washed with a Tris-free 2 M NaCl solution. This approach was motivated by the fact that whenever Tris buffer was retained through the final washing of supercoiled pUC19, prominent Raman bands were observed at 757, 1064, and 1467 cm^{-1}, coincident with the well-known Raman bands of the Tris cation (Figure 4). These interfering Tris Raman bands could be eliminated by a final treatment of the supercoiled plasmid with the same Tris-free high-salt solution used to extract exogenous endonuclease from the linearized plasmid samples. Because the association of Tris cations with DNA can be eliminated by the appropriate treatment of the plasmid with a 2 M NaCl solution, we conclude that Tris−DNA interactions are probably electrostatic in origin and nonspecific. The data of

Figure 4 suggest that in this experiment roughly one Tris ion is present per DNA base pair.

Recently, Stellwagen and co-workers (*21*) reported indistinguishable electrophoretic mobilities of high-molecular weight DNA in Tris-acetate buffers and NaCl solutions of comparable concentrations, suggesting that Tris cations and Na^+ interact similarly with DNA. Because Na^+ is believed to form an extensive counterion layer on the exterior of the DNA helix (*1*, *4*, *21*), we expect similar counterion screening of DNA by Tris cations.

A previous Raman investigation of the supercoiled ColE1 plasmid suggested putative Raman markers of DNA supercoiling near 755, 1060, and 1460 cm^{-1} (*17*). However, these bands coincide closely in wavenumber and intensity with Raman bands of Tris buffer (Figure 4). Indeed, Tris was employed in the previously reported Raman study of the ColE1 plasmid (*17*), and therefore, the unusually strong bands observed near 755, 1060, and 1460 cm^{-1} are likely due to Tris rather than to DNA. The results shown in Figure 4 underscore the importance of avoiding Tris buffers in comparing different forms of DNA by sensitive Raman difference methods. Tris contamination may be particularly problematic when concentrating DNA by ultrafiltration from Tris-buffered solutions.

DISCUSSION

Recent structural studies of supercoiled DNA have focused on large-scale, sequence-specific changes of secondary structure induced by levels of superhelical stress considerably higher than that encountered in vivo. These investigations, which typically involve chemical modification of DNA (*5*), report the formation of (i) left-handed Z-DNA in alternating CG (and CA) sequences (*37*), (ii) cruciforms in palindromic sequences (*38*, *39*), (iii) H-DNA triplexes in homopurine tracts (*40*, *41*), and (iv) underwound DNA in AT-rich sequences (*42*, *43*). Detailed discussions are given in various reviews (*3*, *4*). Less extensively studied are the more subtle changes in B-DNA backbone geometry that may occur in vivo as a result of lower levels of superhelical stress. Raman spectroscopy of native pUC19 permits examination of this question without the need for labeling, ligation, or another form of chemical modification of the DNA substrate. Because pUC19 is only moderately supercoiled ($\sigma = -0.05$) and lacks sequences conducive to the formation of alternative secondary structures, it is well-suited to this analysis.

Supercoiling-Induced Changes in the Structure of pUC19. The Raman difference spectrum between supercoiled and linearized pUC19 (Figure 3, trace D) indicates that supercoiling generates only subtle perturbations to the structure of B-DNA. Here, we consider the structural significance of these Raman results. First, the difference bands at 783 and 814 cm^{-1} coincide with well-characterized markers of the DNA backbone (*8*, *9*, *13*). The small difference trough at 783 cm^{-1} and the corresponding peak at 814 cm^{-1} represent a transfer of intensity from the Raman band near 784 cm^{-1} to the interval of 810−820 cm^{-1}. This spectral change is consistent with a change in the phosphodiester torsion angles α and ζ of the C5′−O5′−⟩−P−⟩−O3′−C3′ network from the *gauche*$^-$/*gauche*$^-$ range to the *gauche*$^-$/*trans* range (*9*−*12*, *25*, *30*) for a small population of pUC19 nucleotide residues. Although Raman markers of cytosine (∼780 cm^{-1}) and thymine (∼790 cm^{-1}) also contribute in the region of the observed difference trough, changes in the pyrimidine ring environments cannot account for the companion difference peak at 814 cm^{-1} (*25*, *32*, *33*). The low amplitudes of the 783 and 814 cm^{-1} difference features (representing a shift of ∼5% of the intensity contributed by the backbone Raman marker at 784 cm^{-1}) imply that no more than ∼250 of the plasmid phosphodiester moieties are affected. This estimate is based on the fact that the parent 784 cm^{-1} band of B-DNA comprises contributions of ∼33% from the backbone and ∼67% from pyrimidines (*8*, *9*, *13*). The observed spectral changes are not likely to be due to fraying or to other effects localized to within one half-turn of each double helix end (*Eco*RI site), because such spectral perturbations could not exceed 0.4% of the parent band intensities.

Second, the peak and trough pair at 1462 and 1489 cm^{-1}, respectively, coincide with well-characterized markers of the state of hydrogen bonding at guanine N7 sites (*19*, *20*, *34*, *44*, *45*). Model compound studies show that the parent guanine band shifts to a lower wavenumber with increasing strength of hydrogen bonding at the N7 acceptor (*19*, *20*, *45*). Thus, the observed difference profile implies that supercoiling results in slightly stronger N7 hydrogen bonding for guanines. The intensity change (≤2%) indicates that only a small subset of dG residues of pUC19 is affected.

Third, the difference trough observed at 1664 cm^{-1} coincides with a strong Raman marker of dT residues that is diagnostic of the state of hydrogen bonding of the thymine C4═O site (*12*, *25*, *35*). Interpretation of this difference feature is complicated, however, by the overlapping contributions expected in the 1600−1680 cm^{-1} interval from H_2O solvent and other DNA base carbonyls. Nevertheless, the simplest interpretation of the 1664 cm^{-1} trough is slightly altered hydrogen bonding of thymine C4═O sites with supercoiling. It should be noted that a perturbation of DNA secondary structure can result not only in a shift in the center of a Raman marker band (leading to a peak and trough couplet in the difference spectrum) but also in a decrease or increase in peak intensity without a shift in the band center (*8*−*13*).

It is of interest that all of the difference bands of Figure 3D can be attributed to structural adjustments affecting either the DNA backbone or the local environment of base sites lining the major groove (Table 1). A corollary to these results is the fact that pUC19 accommodates its supercoiling free energy $\{\Delta G_{Lk} = [(1050RT)/N]\Delta Lk^2 = 51.2$ kcal/mol of DNA$\}$ without radically compromising the canonical B-DNA conformation. We conclude further that for covalently closed DNA with sequence characteristics similar to those of pUC19 an elevation of the free energy by ∼0.019 kcal/bp is not sufficient to destabilize the B-DNA conformation in favor of known alternative secondary structures for at least 95% of the base pairs.

Comparison with Other Supercoiled Plasmids. Although Raman spectroscopy has been employed previously to investigate the negatively supercoiled plasmids pBR322 (4362 bp, $\sigma = -0.069$) (*15*, *16*, *18*) and ColE1 (6646 bp, $\sigma = -0.078$) (*17*), less extensive experimental data were obtained and small intensity changes (≤5%) were not resolved. In the case of pBR322, neither Raman intensity changes nor frequency shifts with supercoiling could be demonstrated from the raw experimental data (*16*, *18*). Yet,

spectral markers of supercoiling were proposed at 810 and 818 cm^{-1} on the basis of deconvolution and curve-fitting analyses of computationally smoothed data (*18*). Surprisingly, the wavenumber range (810−818 cm^{-1}) of the proposed intensity increase for pBR322 is similar to one of the difference features (814 cm^{-1}) observed here for pUC19 (Figure 3). The apparent wavenumber agreement may be fortuitous, because no corresponding intensity decrease near 784 cm^{-1} was reported for pBR322 (*18*). Furthermore, in the previous study, the deconvolution result was attributed to a supercoiling-induced change in sugar puckering from C2′-*endo* to C3′-*endo* for a subset of the pBR322 deoxynucleosides. The data of Figure 3 show convincingly, however, that no deoxynucleoside marker in the 600−750 cm^{-1} region (*13*) is altered significantly by supercoiling in pUC19. Accordingly, as noted above, we attribute the Raman spectral perturbations observed for pUC19 to (i) an intramolecular conformational change localized in DNA phosphodiester moieties (*gauche*$^-$/*gauche*$^-$ → *gauche*$^-$/*trans*) and (ii) concomitant perturbation of hydrogen bonding environments at base sites that line the major groove of B-DNA. We find no evidence of changes in deoxyribosyl pucker. We also note that neither computational smoothing nor curve fitting has been imposed to detect the supercoiling-induced changes to topoisomer-specific Raman signatures of pUC19 (Figure 3).

In the investigation of ColE1 by Raman spectroscopy (*17*), extraordinarily intense Raman markers of supercoiling were proposed at 755, 1060, and 1460 cm^{-1}. However, as seen in Figure 4A and noted in the Results, these proposed Raman markers of DNA supercoiling can be ascribed entirely to contributions from Tris cations associated with the DNA solution.

It is often assumed that buffers used to maintain physiological pH in vitro do not form stable complexes with DNA. However, specific and stable complexes have been proposed between linear DNA and borate ions in Tris-borate buffers (*21*). The data of Figure 4 suggest at least the possibility of nonspecific association of Tris cations with supercoiled DNA. Because the presently observed Tris contributions to the DNA Raman spectrum can be eliminated by washing the DNA with a 2 M NaCl solution, the association of Tris with DNA is presumed to be electrostatic in origin. The Raman markers of DNA isolated from the Tris-buffered solution (Figure 4A) are indistinguishable from those of DNA isolated from Tris-free solution (Figure 3A), indicating no significant perturbation to the B-form secondary structure from the Tris counterions. On the basis of these findings, we conclude that DNA samples intended for sensitive Raman difference spectral analyses should not be exposed to Tris buffers unless followed by appropriate washing with high-salt solutions.

Compatibility of Raman and CD Profiles of Supercoiled DNA. The CD spectrum of supercoiled pUC19 (Figure 2) exhibits no major change from the well-established ellipticity profile of B-DNA. The small and uncompensated increase in ellipticity near 277 nm relative to the linearized plasmid is attributed to a small decrease in average helical twist without significant disruption of base stacking or base pairing. Thus, the CD and Raman spectra are consistent in indicating the conservation of B-form secondary structure for pUC19 at a superhelical density σ of −0.05. Alternative secondary structures, such as A-, Z-, and H-DNA and branched forms of DNA, are not evident under these conditions.

Negative-stain electron microscopy of supercoiled pUC19 (*46*) and Monte Carlo simulations (*1*) of supercoiled DNA at moderate superhelical density also indicate predominantly unbranched B-DNA, in agreement with the spectroscopic results presented here. In contrast to plasmids of high superhelical density that are proposed to undergo major localized changes in secondary structure (*18*), pUC19 appears to accommodate moderate superhelical stress through small structural adjustments that may be distributed throughout the sequence.

Our results are also in accord with earlier CD studies of topoisomers of the pBR322 plasmid (*18*) and the replicative form of φX174 DNA (*47*). These studies show an increase in CD ellipticity near 275 nm with negative supercoiling and a corresponding decrease with positive supercoiling, attributed to a decrease and an increase, respectively, in helical twist. The ellipticity change at 275 nm is reported to depend linearly on superhelical density within the range of −0.05 to 0.05 (*18*). Outside of this range, however, DNA branching or major secondary structural changes are believed to account for the more radical differences observed in CD signatures (*1*, *18*).

Significance for Activation of Transcription. Transcriptional activation of promoters in both prokaryotes and eukaryotes is strongly dependent on the negative superhelical density of chromosomal DNA (*2*, *48*−*51*). Moderate supercoiling ($\sigma = -0.05 \pm 0.01$) is important for optimal transcription (*48*) and is stringently controlled in vivo by topoisomerases and gyrases (*14*). Further increases in superhelicity inhibit transcription (*48*). Our study shows that moderate supercoiling ($\sigma = -0.05$) of pUC19 perturbs only slightly the canonical B-DNA structure associated with the relaxed form, and does not introduce significant branching or known alternative secondary structures.

Transcription factor recognition of structurally perturbed B-DNA has been proposed as a critical step in transcriptional activation (*49*, *50*, *52*). In support of this hypothesis, it has been noted that replacement of the DNA binding site of integration host factor (IHF) in the *E. coli* ilvPG promoter with the binding site of the mammalian lymphoid enhancer-binding factor-1 (LEF-1) does not abolish transcription (*49*). Both IHF and LEF-1 are known to induce strong bends in their DNA binding sites. Evidently, a structural feature common to both transcription factor-bound DNA sites, rather than a specific interaction involving the transcription factor and RNA polymerase, is required for activation. Related studies of the ilvPG promoter region suggest that a "destabilized" backbone is induced by superhelical stress (*50*) and that this perturbed B-DNA conformation is propagated downstream upon transcription factor binding. Such a mechanism, which is supported by studies of other prokaryotic (*53*, *54*) and eukaryotic promoters (*51*), is also in accord with the results presented here.

The *gauche*$^-$/*trans* phosphodiester conformation, sometimes termed B_{II}-DNA (*55*), is recognized as an important structural modification of B-DNA that may be involved in transcriptional activation (*50*). These results support this hypothesis and indicate the potential of Raman difference spectroscopy in detecting the B_{II} variant. A similar Raman approach should be effective for investigating DNA−

transcription factor complexes. Recent Raman studies of DNA complexes of the transcriptional activators GCN4 (*20*) and hSRY (*19*) provide specific applications. The long-range goal of this work is to establish an extensive library of Raman markers of both perturbed and canonical DNA structures implicated in protein recognition. In principle, such a library could be used to identify specific DNA−protein binding motifs and to classify patterns of structural change (including superhelical stress) imposed by gene regulatory proteins. Although high-resolution structural methods can provide three-dimensional structures of small DNA−protein complexes in exquisite detail, they are not generally as well suited as Raman spectroscopy to the investigation of supercoiled plasmids and other large DNA molecules in complexes with regulatory proteins.

REFERENCES

1. Vologodskii, A. V., and Cozzarelli, N. R. (1994) *Annu. Rev. Biophys. Biomol. Struct. 23*, 609−643.
2. Harland, R. M., Weintraub, H., and McKnight, S. L. (1983) *Nature 302*, 38−43.
3. Wells, R. D. (1988) *J. Biol. Chem. 263*, 1095−1098.
4. Strick, T. R., Allemand, J. F., Bensimon, D., and Croquette, V. (2000) *Annu. Rev. Biophys. Biomol. Struct. 29*, 523−543.
5. Lilley, D. M. (1992) *Methods Enzymol. 212*, 133−139.
6. Boles, T. C., White, J. H., and Cozzarelli, N. R. (1990) *J. Mol. Biol. 213*, 931−951.
7. Overman, S. A., Aubrey, K. L., Reilly, K. E., Osman, O., Hayes, S. J., Serwer, P., and Thomas, G. J., Jr. (1998) *Biospectroscopy 4*, S47−S56.
8. Erfurth, S. C., Kiser, E. J., and Peticolas, W. L. (1972) *Proc. Natl. Acad. Sci. U.S.A. 69*, 938−941.
9. Prescott, B., Steinmetz, W., and Thomas, G. J., Jr. (1984) *Biopolymers 23*, 235−256.
10. Benevides, J. M., Wang, A. H. J., Rich, A., Kyogoku, Y., van der Marel, G. A., van Boom, J. H., and Thomas, G. J., Jr. (1986) *Biochemistry 25*, 41−50.
11. Benevides, J. M., Wang, A. H. J., van der Marel, G. A., van Boom, J. H., and Thomas, G. J., Jr. (1988) *Biochemistry 27*, 931−938.
12. Katahira, M., Nishimura, Y., Tsuboi, M., Sato, T., Mitsui, Y., and Iitaka, Y. (1986) *Biochim. Biophys. Acta 867*, 256−267.
13. Thomas, G. J., Jr., and Tsuboi, M. (1993) Raman Spectroscopy of Nucleic Acids and Their Complexes, in *Advances in Biophysical Chemistry* (Bush, C. A., Ed.) Vol. 3, pp 1−70, JAI Press, Inc., Greenwich, CT.
14. LaMarr, W. A., Sandman, K. M., Reeve, J. N., and Dedon, P. C. (1997) *Nucleic Acids Res. 25*, 1660−1661.
15. Hayashi, H., Nishimura, Y., Tsuboi, M., Sekimizu, K., Nakanishi, Y., and Natori, S. (1985) *Biopolymers 24*, 1107−1111.
16. Vasmel, H. (1985) *Biopolymers 24*, 1001−1008.
17. Christens-Barry, W. A., Martin, J. C., and Lebowitz, J. (1989) *Biopolymers 28*, 1515−1526.
18. Brahms, S., Nakasu, S., Kikuchi, A., and Brahms, J. G. (1989) *Eur. J. Biochem. 184*, 297−303.
19. Benevides, J. M., Chan, G., Lu, X.-J., Olson, W. K., Weiss, M. A., and Thomas, G. J., Jr. (2000) *Biochemistry 39*, 537−547.
20. Benevides, J. M., Li, T., Lu, X.-J., Srinivasan, A. R., Olson, W. K., Weiss, M. A., and Thomas, G. J., Jr. (2000) *Biochemistry 39*, 548−556.
21. Stellwagen, N. C., Gelfi, C., and Righetti, P. G. (2000) *Biopolymers 54*, 137−142.
22. Yang, X. M. (1992) *J. Biotechnol. 23*, 271−289.
23. Sambrook, J., Fritsch, E. F., and Maniatis, T. (1989) *Molecular Cloning: A Laboratory Manual*, Cold Spring Harbor Laboratory Press, Plainview, NY.
24. Thomas, G. J., Jr., and Barylski, J. (1970) *Appl. Spectrosc. 24*, 463−464.
25. Movileanu, L., Benevides, J. M., and Thomas, G. J., Jr. (1999) *J. Raman Spectrosc. 30*, 637−649.
26. Zivanovic, Y., Goulet, I., and Prunell, A. (1986) *J. Mol. Biol. 192*, 645−660.
27. Woody, R. W. (1995) *Methods Enzymol. 246*, 34−71.
28. Benevides, J. M., and Thomas, G. J., Jr. (1983) *Nucleic Acids Res. 11*, 5747−5761.
29. Duguid, J., Bloomfield, V. A., Benevides, J. M., and Thomas, G. J., Jr. (1993) *Biophys. J. 65*, 1916−1928.
30. Deng, H., Bloomfield, V. A., Benevides, J. M., and Thomas, G. J., Jr. (1999) *Biopolymers 50*, 656−666.
31. Duguid, J., Bloomfield, V. A., Benevides, J. M., and Thomas, G. J., Jr. (1996) *Biophys. J. 71*, 3350−3360.
32. Benevides, J. M., Kukolj, G., Autexier, C., Aubrey, K. L., DuBow, M. S., and Thomas, G. J., Jr. (1994) *Biochemistry 33*, 10701−10710.
33. Small, E. W., and Peticolas, W. L. (1971) *Biopolymers 10*, 1377−1418.
34. Nishimura, Y., Tsuboi, M., Nakano, T., Higuchi, S., Sato, T., Shida, T., Uesugi, S., Ohtsuka, E., and Ikehara, M. (1983) *Nucleic Acids Res. 11*, 1579−1588.
35. Thomas, G. J., Jr., Benevides, J. M., Overman, S. A., Ueda, T., Ushizawa, K., Saitoh, M., and Tsuboi, M. (1995) *Biophys. J. 68*, 1073−1088.
36. Benevides, J. M., Stow, P. L., Ilag, L. L., Incardona, N. L., and Thomas, G. J., Jr. (1991) *Biochemistry 30*, 4855−4863.
37. Giaever, G. N., Snyder, L., and Wang, J. C. (1988) *Biophys. Chem. 29*, 7−15.
38. Haniford, D. B., and Pulleyblank, D. E. (1985) *Nucleic Acids Res. 13*, 4343−4363.
39. Murchie, A. I., and Lilley, D. M. (1987) *Nucleic Acids Res. 15*, 9641−9654.
40. Wohlrab, F., McLean, M. J., and Wells, R. D. (1987) *J. Biol. Chem. 262*, 6407−6416.
41. Belotserkovskii, B. P., Veselkov, A. G., Filippov, S. A., Dobrynin, V. N., Mirkin, S. M., and Frank-Kamenetskii, M. D. (1990) *Nucleic Acids Res. 18*, 6621−6624.
42. Greaves, D. R., Patient, R. K., and Lilley, D. M. (1985) *J. Mol. Biol. 185*, 461−478.
43. Kowalski, D., Natale, D. A., and Eddy, M. J. (1988) *Proc. Natl. Acad. Sci. U.S.A. 85*, 9464−9468.
44. Lord, R. C., and Thomas, G. J., Jr. (1967) *Spectrochim. Acta 23A*, 2551−2591.
45. Nishimura, Y., Tsuboi, M., Sato, T., and Aoki, K. (1986) *J. Mol. Struct. 146*, 123−153.
46. Adrian, M., Heggeler-Bordier, B., Wahli, W., Stasiak, A. Z., Stasiak, A., and Dubochet, J. (1990) *EMBO J. 9*, 4551−4554.
47. MacDermott, A. J., and Drake, A. F. (1986) *Stud. Biophys. 115*, 59−67.
48. Brahms, J. G., Dargouge, O., Brahms, S., Ohara, Y., and Vagner, V. (1985) *J. Mol. Biol. 181*, 455−465.
49. Parekh, B. S., and Hatfield, G. W. (1996) *Proc. Natl. Acad. Sci. U.S.A. 93*, 1173−1177.
50. Sheridan, S. D., Benham, C. J., and Hatfield, G. W. (1998) *J. Biol. Chem. 273*, 21298−21308.
51. Shao, W., Lee, A. Y., Gulnik, S., Gustchina, E., Liu, Y. L., Kung, H., and Erickson, J. W. (2000) *FEBS Lett. 473*, 363−369.
52. Parekh, B. S., Sheridan, S. D., and Hatfield, G. W. (1996) *J. Biol. Chem. 271*, 20258−20264.
53. Chen, Y. C., and Jeng, S. T. (2000) *Biosci., Biotechnol., Biochem. 64*, 1126−1132.
54. Sawers, G. (2001) *Mol. Microbiol. 39*, 1285−1298.
55. Gorenstein, D. G. (1992) *Methods Enzymol. 211*, 254−286.

BI011004Z